Bias-voltage dependent STM images from the 2–fold surface of the icosahedral Ag-In-Yb quasicrystal

Dominic Burnie[1] Sam Coates[1,2], Ronan McGrath[1], and Hem Raj Sharma[1]

[1]Surface Science Research Centre, Department of Physics, University of Liverpool, Liverpool, L69 3BX, UK

[2]Department of Materials Science and Technology, Tokyo University of Science, 6 Chome–3–1 Niijuku, Katsushika City, Tokyo 125-8585

E-mail: H.R.Sharma@liv.ac.uk

Abstract. The 2–fold surface of the icosahedral (i–) Ag–In–Yb quasicrystal has been investigated using scanning tunnelling microscopy (STM). STM data reveals a bias-voltage dependency. At high positive bias, a row-structure is observed, with brighter protrusions lying within the rows. At negative bias, new protrusions appear while the size of the original protrusions decreases and a different set of vertical rows are observed. The STM features at both positive and negative bias polarities can be related to bulk planes intersecting the centre of the Tsai-type clusters that are the building blocks of the bulk. The bias-dependency can be explained by the change in contribution in tunneling current from Yb and Ag/In that is expected from density of states calculations.

1. Introduction

The atomic structure of the high-symmetry (2–, 3–, and 5–fold) surfaces of the i–Ag–In–Yb system has been well-studied. The surfaces are found to be terminated at bulk planes intersecting the centre of the Tsai-type clusters, the building block of the system [1, 2, 3, 4, 5]. In the 3–fold and 5–fold cases, atomic resolution has been achieved in STM, so that specific motifs in the model can be matched to those observed by STM. Morphological dependence on bias voltage was observed on the 5-fold surface. In STM, positive sample bias probes unoccupied states and negative bias probes occupied states. Yb sites were preferentially observed on the 5–fold surface with positive bias [2], a phenomena expected due to the domination of the Yb $4d$ level in the unoccupied density of states [6, 7]. Likewise, achieving atomic resolution on the 3–fold surface was observed to be sensitive towards tip bias [3].

In the previous report on 2–fold Ag–In–Yb, enhanced resolution by STM was obtained at positive bias, but no clear bias-dependency was observed [4]. In this report we show higher resolution images, where bias-dependency is clearly observed. Features seen at both positive and negative bias are linked to Ag/In–Yb model planes truncated at cluster centres.

2. Methods

An i–Ag–In–Yb quasicrystal with a surface perpendicular to its 2–fold rotational axis was polished with diamond paste (6–0.25 μm) before washing with methanol in an ultrasonic bath.

Upon insertion into an ultra–high vacuum (UHV) chamber, the surface was further cleaned with cycles of sputter–annealing. Each sputter used Ar^+ for 30 minutes, before annealing at 425°C for 2 hours. STM was used to probe the surface morphology. The bias voltage polarity stated in this report is with respect to the sample

3. Results

We measured STM from the clean 2–fold Ag–In–Yb surface at various bias voltages (from +2.5 V to -2.5 V). Data was taken from the same area on the surface with the same tip condition. As such, direct comparison between each data set was possible. Here, we will discuss a representative image of each bias polarity (+2.5 V and -0.8 V). The 2–fold surface contains all three high-symmetry directions of the bulk vectors (i.e. 2–fold, 3–fold, 5–fold). These are shown in Figure 1(h). The STM images presented here will be oriented in the same fashion for comparison. The high symmetry directions of the STM images were determined from the Fourier transform patterns of the images.

Figure 1(a) shows an STM image at +2.5 V. A row-structure with intermediate contrast is observed along one of the 2–fold axes (vertical direction in Figure). In addition to this, a range of bright protrusions can be seen. They display alignment along the 2–fold and 5–fold axes. Dimmer features often link closely spaced bright protrusions in the 5–fold direction. Examples of arrangements in this direction have been highlighted in green. The separations between these features exhibit a segment of the Fibonacci chain, where the ratio between long (L) and short (S) is equal to τ (= 1.618..., the golden ratio).

Alignment of protrusions along high-symmetry axes often results in the formation of diamond-like features. A set of four such diamonds are shown in Figure 1(a) and its inset, where the protrusions lie at the vertices of the diamonds. The average small and large diagonal of the diamond are 2.57±0.08 nm and 4.19±0.02 nm respectively. The ratio of these two values is $\approx \tau$. Protrusions are observed to reside in between vertical rows (highlighted in Figure 1(a)), where dimmer features link the vertices along the diamond edges.

The autocorrelation of Figure 1(a) (shown in Figure 1(b)) was used to calculate the separation of the vertical rows. Clear rows are visible along the 2–fold axes (highlighted by vertical solid blue lines). The average separation between these rows is 1.32 ± 0.04 nm. The same separation was used for the rows highlighted in Figure 1(a). Diamond-like features with a protrusion at each vertex are visible also in the autocorrelation function. Four diamonds of the same dimensions and geometry as in Figure 1(a) are highlighted in Figure 1(b). Features arranged along the 5-fold direction with separations following a Fibonacci chain are again highlighted in green.

The fast Fourier transform (FFT) of Figure 1(a) is shown in Figure 1(c). A set of τ-scaled concentric rectangles with aspect ratio also equal to τ have been overlaid. Diffraction maxima are located at the vertices and edges of each rectangle, confirming the quasicrystalline 2-fold symmetry of the surface. Different colours correspond to spots along three high symmetry directions (blue: 2-fold, pink: 3-fold, green: 5-fold). The corresponding real-space separation between the spots along the horizontal 2-fold direction matches the separation of horizontal rows in Figure 1(a) and (b). Each maximum may be indexed using the four basis vectors marked in blue in Figure 1(c).

We now discuss a possible explanation for the features observed by STM. This involves comparison with the model bulk structure. Figure 1(d) shows a model 2–fold Ag/In–Yb plane, formed via a bulk truncation through i–Ag/In–Yb cluster centres. Different colours correspond to atoms belonging to different shells of the Tsai-type cluster (light green: third shell Yb, dark green: glue Yb, purple: second shell Ag/In, light pink: fourth shell Ag/In and dark pink: fifth shell Ag/In.) First shell Ag/In atomic positions have been omitted. The protrusions observed by STM may be understood in terms of two distinct sites; a triangle of three Yb atoms surrounding one fourth shell Ag/In atomic position and a square of four Yb atoms surrounding a fourth shell

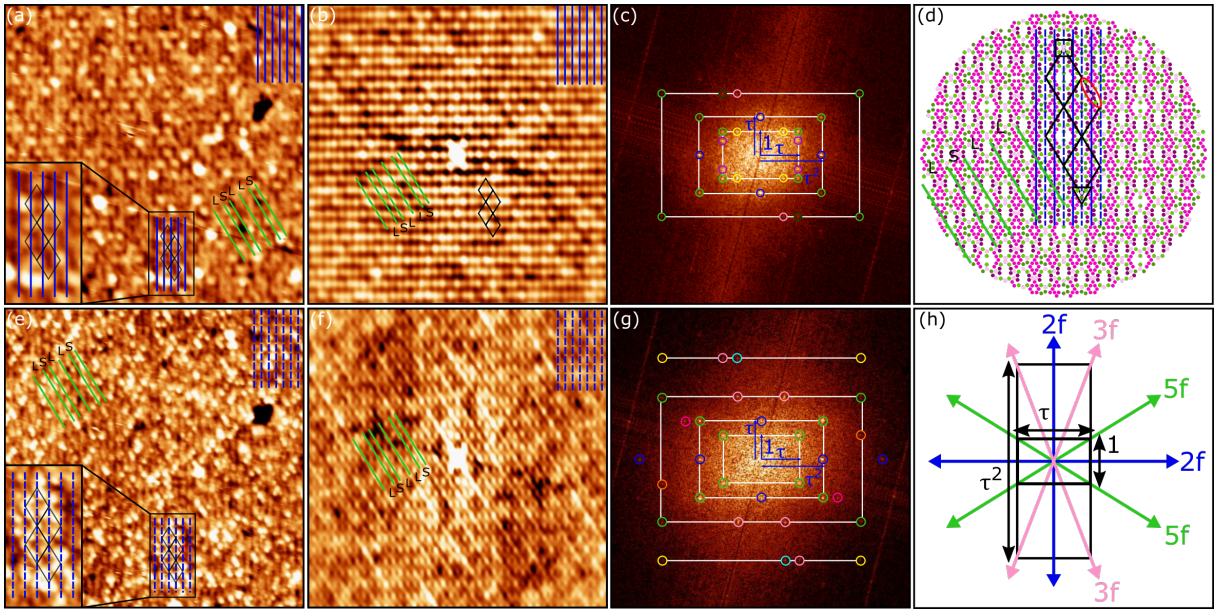

Figure 1. (a) STM image of the 2–fold surface at +2.5 V (54 nm × 54 nm). Inset: marked section in a magnified view. (b) The autocorrelation pattern of (a). (c) The fast Fourier transform (FFT) of (a). Blue, pink and green circled spots lie along the 2-fold, 3-fold and 5-fold high-symmetry directions respectively. (d) A model atomic plane intersecting the cluster centres (20 nm × 20 nm, light green: third shell Yb, dark green: glue Yb, purple: second shell Ag/In, light pink: fourth shell Ag/In and dark pink: fifth shell Ag/In). (e) An STM image of the 2–fold surface at -0.8 V (54 nm × 54 nm). Inset: marked section in a magnified view. (f) The autocorrelation pattern of (e). (g) The FFT of (e). Colour scheme is the same as in (c). (h) High-symmetry directions of the 2-fold surface, as determined from the FFT.

dimer. An example of each is highlighted by a triangle and square respectively in Figure 1(d).

Like the protrusions, these sites show clear alignment along the 2–fold and 5–fold axes. A set of diamond-like motifs with vertices formed by these sites are highlighted in Figure 1(d). Their dimensions and geometry match those marked in Figure 1(a). Closely spaced second and fourth shell dimers reside along the edges of each diamond, linking the Yb features along the 5–fold axes. One is highlighted in red. This is consistent with the dimmer 'linking' features observed in between protrusions by STM.

The vertical rows observed by STM may be linked to the atomic rows marked by blue solid lines in Figure 1(d). These rows contain atoms belonging to the fourth and fifth Ag/In shell. The average vertical row-separation is 1.33 ± 0.09 nm. This is consistent with the row-separation observed experimentally. As in STM, these rows pass through the mid-edges of the diamond features. Previous STM measurements at positive bias also identified a contribution from these rows [4].

Figure 1(e) shows an STM image at -0.8 V. A marked area of this image is shown in a magnified scale in the inset. A set of diamonds displaying the same dimensions, geometry and location as in Figure 1(a) have been overlaid on Figure 1(e). The protrusions observed at +2.5 V are still observed at the vertices of each diamond, but their size decreases. New protrusions of comparable size and contrast are also observed along the diamond edges, displaying a pronounced alignment of protrusions along a 5–fold axis. Examples have been highlighted in green in Figure 1(e). The separations between these features exhibit a segment of the Fibonacci chain. Vertical rows are observed also at -0.8 V but in contrast to those of +2.5 V they pass through the

vertices of the diamond (vertical dashed blue lines). This suggests these rows are not the same vertical rows observed at +2.5 V. However, the separation of these new rows is same as that observed at +2.5 V. This separation was determined from the autocorrelation pattern of the STM image (Figure 1(f)). In the autocorrelation pattern, row-like structures along the 5-fold axes are dominant. Separations distances following a Fibonacci chain are again highlighted in green in Figure 1(f).

The FFT of Figure 1(e) is shown in Figure 1(g). Once again, each diffraction maximum may be accounted for using the same two basis vectors. However, maxima along 5-fold axes have been enhanced in intensity. This is consistent with the observed enhancement of protrusions along the 5-fold direction.

The protrusions observed at the vertices of diamonds can be understood in terms of the same sites described for +2.5 V (i.e. Yb surrounding fourth shell Ag/In sites). The additional protrusions observed at -0.8 V can be related to the fourth and fifth shell Ag/In atoms (highlighted in red in Figure 1(d)). The vertical rows at -0.8 V corresponds to Yb rich rows in the model (marked in dashed blue lines in Figure 1(d)). The average separation between these rows matches the experimental value.

The change in contrasts of different sites between each bias can be explained in terms of partial density of states calculations [6, 7]. It is expected from calculations that tunneling current contribution from Yb outweighs that for Ag/In at higher positive bias. At negative bias, the contribution from each becomes comparable [6]. This supports the suggestion that Yb features contribute to the large bright protrusions observed at positive bias, while at negative bias Ag/In sites equally contributes producing the additional protrusion. The row structure observed at both biases can be explained by the same argument.

4. Conclusions

We have shown here the STM images from the 2–fold Ag–In–Yb surface are bias voltage dependent. At higher positive bias, a vertical row-structure is observed. A range of protrusions reside within this row-structure, displaying alignment along the 2-fold and 5-fold axes. At negative bias, a different set of vertical rows are seen. The size of the protrusions at negative bias is reduced, and additional protrusions appear. The difference can be explained by enhanced contribution in tunneling current from Yb sites over Ag/In sites at positive bias and equal contribution from both Yb and Ag/In sites at negative bias, which is expected from partial density of states calculation.

References

[1] H. R. Sharma, M. Shimoda, S. Ohhashi, and A. P. Tsai. First UHV surface studies of single-grain icosahedral Ag–In–Yb quasicrystal. *Philosophical Magazine*, 87(18-21):2989–2994, 2007.

[2] H. R. Sharma, M. Shimoda, K. Sagisaka, H. Takakura, J. A. Smerdon, P. J. Nugent, R. McGrath, D. Fujita, S. Ohhashi, and A. P. Tsai. Structure of the fivefold surface of the Ag-In-Yb icosahedral quasicrystal. *Phys. Rev. B*, 80(12):121401, 2009.

[3] C. Cui, P. J. Nugent, M. Shimoda, J. Ledieu, V. Fourne, A. P. Tsai, R. McGrath, and H. R. Sharma. The atomic structure of the threefold surface of the icosahedral AgInYb quasicrystal. *Journal of Physics: Condensed Matter*, 24(44):445011, 2012.

[4] C. Cui, P. J. Nugent, M. Shimoda, J. Ledieu, V. Fournée, A. P. Tsai, R. McGrath, and H. R. Sharma. Structure of the twofold surface of the icosahedral Ag–In–Yb quasicrystal. *Journal of Physics: Condensed Matter*, 26(1):015001, 2013.

[5] H. Takakura, C. P. Gómez, A. Yamamoto, M. de Boissieu, and A. P. Tsai. Atomic structure of the binary icosahedral Yb–Cd quasicrystal. *Nature Materials*, 6(1):58, 2007.

[6] H. R. Sharma, G. Simutis, V. R. Dhanak, P. J. Nugent, C. Cui, M. Shimoda, R. McGrath, A. P. Tsai, and Y. Ishii. Valence band structure of the icosahedral Ag-In-Yb quasicrystal. *Physical Review B*, 81(10):104205, 2010.

[7] Y. Ishii and T. Fujiwara. Hybridization mechanism for cohesion of Cd-based quasicrystals. *Phys. Rev. Lett.*, 87(20):206408, 2001.